The potential of *in situ* cosmogenic ^{14}CO in ice cores as a proxy for galactic cosmic ray flux variations

Vasilii V. Petrenko[1], Segev BenZvi[2], Michael Dyonisius[1,a], Benjamin Hmiel[1,b], Andrew M. Smith[3] and Christo Buizert[4]

[1]Department of Earth and Environmental Sciences, University of Rochester, Rochester, NY, USA
[2]Department of Physics and Astronomy, University of Rochester, Rochester, NY, USA
[3]Centre for Accelerator Science, Australian Nuclear Science and Technology Organization, Lucas Heights, NSW, Australia
[4]College of Earth, Ocean and Atmospheric Sciences, Oregon State University, Corvallis, OR, USA
[a]present address: Institute of Arctic and Alpine Research, University of Colorado Boulder, Boulder, CO, USA
[b]present address: Air Pollution Control Division, Colorado Department of Public Health and the Environment, Glendale, CO, USA

Correspondence to: Vasilii V. Petrenko (vasilii.petrenko@rochester.edu)

Abstract

Galactic cosmic rays (GCRs) interact with matter in the atmosphere and at the surface of the Earth to produce a range of cosmogenic nuclides. Measurements of cosmogenic nuclides produced in surface rocks have been used to study past land ice extent as well as to estimate erosion rates. Because the GCR flux reaching the Earth is modulated by magnetic fields (solar and Earth's), records of cosmogenic nuclides produced in the atmosphere have also been used for studies of past solar activity. Studies utilizing cosmogenic nuclides assume that the GCR flux is constant in time, but this assumption may be uncertain by 30% or more. Here we propose that measurements of ^{14}C of carbon monoxide (^{14}CO) in ice cores at low-accumulation sites can be used as a proxy for variations in GCR flux on timescales of several thousand years. At low-accumulation ice core sites, ^{14}CO in ice below the firn zone originates almost entirely from *in situ* cosmogenic production by deep-penetrating secondary cosmic ray muons. The flux of such muons is almost insensitive to solar and geomagnetic variations, and depends only on the primary GCR flux intensity. We use an empirically-constrained model of *in situ* cosmogenic ^{14}CO production in ice in combination with a statistical analysis to explore the sensitivity of ice core ^{14}CO measurements at Dome C, Antarctica to variations in the GCR flux over the past $\approx$7000 years. We find that Dome C ^{14}CO measurements would be able to detect a linear change of 4% over 7 ka, a step increase of 4% at 3.5 ka or a transient 100-year spike of 250% at 3.5 ka at the 3 σ significance level. The ice core ^{14}CO proxy therefore appears promising for the purpose of providing a high-precision test of the assumption of GCR flux constancy over the Holocene.

1 Introduction

The galactic cosmic ray (GCR) flux at Earth is modulated by both the geomagnetic and the heliospheric (solar) magnetic fields. The heliospheric magnetic field strength is linked to solar activity and solar irradiance (e.g., Wu et al., 2018b; Steinhilber et al., 2009), with irradiance being a key climate driver. This has enabled the use of

records of past cosmogenic nuclide production rates for studies of past solar variability (e.g., Adolphi et al., 2014; Bard et al., 2000; Steinhilber et al., 2009; Usoskin et al., 2016; Usoskin, 2023). The two main nuclides that have been used for these studies are ^{14}C (mainly from tree rings, which record atmospheric $^{14}C/^{12}C$ ratio) and ^{10}Be (from ice cores, which record the flux of ^{10}Be at the snow deposition site). Measurements of cosmogenic nuclides have also been used extensively to study processes at the Earth's surface, such as the timing of glacial advance and retreat (e.g., Balco, 2020). In these applications, nuclides such as ^{10}Be, ^{14}C, ^{26}Al and ^{36}Cl that are produced *in situ* in surface rocks are of interest.

Cosmogenic nuclide-based reconstructions of past solar activity and ice extent have relied on the assumption that the GCR flux is constant in time (e.g., Balco, 2011; Gosse and Phillips, 2001; Muscheler, 2013). Measurements of cosmogenic radionuclides in meteorites provide arguably the strongest support for this assumption (e.g., Smith et al., 2019; Wieler et al., 2013). However, a number of important uncertainties are involved when interpreting these measurements, including meteoroid orbits, solar modulation of the GCR flux and break-up of meteoroids / fresh surface exposure on entry into the atmosphere. A review by Wieler et al. (2013) concluded that while overall the meteorite evidence indicates that the GCR flux is constant, this assumption is uncertain by 30% or more. Measurements of cosmogenic nuclides in lunar rocks also indirectly indicate that the GCR flux could have been constant on million-year timescales, although there is still a confounding influence of solar modulation (e.g., Poluianov et al., 2018). Records of $^{10}Be/^9Be$ ratios in oceanic sediments and iron-manganese crusts (Willenbring and von Blanckenburg, 2010) have also been used to argue that the GCR flux is approximately constant on million-year timescales (Wieler et al., 2013). However, this approach also involves multiple confounding factors, such as solar and geomagnetic modulation of the GCR flux and ^{10}Be transport, deposition and oceanic cycling. Results from studies that have used cosmogenic ^{14}C and ^{10}Be to examine past solar activity also assume that there were no large changes in the GCR flux in the past few millennia (e.g., Knudsen et al., 2009; Steinhilber et al., 2012; Wu et al., 2018a). However, again, inferences about the GCR flux from such records are complicated by solar and geomagnetic modulation (e.g., Knudsen et al., 2008), carbon cycle (for ^{14}C, e.g., Muscheler et al., 2007) and transport and deposition effects (for ^{10}Be; e.g., Field et al., 2006).

Theoretical considerations also generally support the assumption that the GCR flux is constant, though small anisotropies are expected due to the effect of the nearest sources of GCRs and the diffusive propagation of cosmic rays in the galaxy (Erlykin and Wolfendale, 2006; Blasi and Amato, 2012; Ahlers and Mertsch, 2015; Mertsch and Funk, 2015). At energies above 100 GeV, the GCR flux at Earth today is isotropic to within 1 part in 1000, with the residual anisotropy characterized by a dipole plus statistically significant components on angular scales as small as 5 degrees (e.g., Abeysekara et al., 2019 and references therein). The observations indicate that cosmic ray transport is dominated by diffusion in galactic magnetic fields, which should dampen the contributions of spatial and temporal point sources of cosmic rays. Nevertheless, significant GCR flux variations are in principle possible even on sub-millennial timescales. For example, Melott et al. (2017) and Thomas et al. (2016) consider the terrestrial effects of a supernova 50 parsecs from Earth and estimate that the production rate of atmospheric muons could increase by up to several orders of magnitude depending on how accelerated GCRs propagate through nearby galactic magnetic fields. While the predictions of such models should be understood to represent the extreme upper limit of possible effects, a

number of observations suggest that supernova explosions in our galactic neighborhood do produce measurable effects on the local properties of GCRs. Such observations include the part-per-mille dipole anisotropy in the cosmic ray flux above 1 TeV (e.g., Abeysekara et al., 2019; Ahlers and Mertsch, 2015; Blasi and Amato, 2012; Erlykin and Wolfendale, 2006), the fluxes of positrons and antiprotons above 20 GeV and heavy nuclei above 1 TeV (e.g., Kachelriess et al., 2015), and measurements of ^{60}Fe in ocean sediments (Wallner et al., 2016) and Antarctic snow (Koll et al., 2019). Thus, high-precision tests of GCR flux variations that are free of the confounding factors discussed above for meteorites and for cosmogenic ^{10}Be and ^{14}C produced in the atmosphere would be valuable.

2 Systematics of *in situ* cosmogenic ^{14}CO in glacial ice

2.1 Overview of ^{14}CO in glacial ice

We first provide an overview of the current understanding of the processes that control the abundance of *in situ* cosmogenic ^{14}CO in glacial ice, which is needed to understand how the ice core ^{14}CO proxy for GCR flux variations works. ^{14}C in glacial ice originates from trapping of ^{14}C-containing atmospheric gases such as carbon dioxide (CO_2), methane (CH_4) and carbon monoxide (CO) as well as from *in situ* cosmogenic production. *In situ* ^{14}C is produced in glacial ice and firn via interactions of secondary cosmic ray neutrons and muons with ^{16}O in the ice grains (Fig 1a) (e.g., Lal et al., 1997; Petrenko et al., 2016; van der Kemp et al., 2002). Once produced, this ^{14}C reacts rapidly to form predominantly $^{14}CO_2$ and ^{14}CO, with a small amount of $^{14}CH_4$ and possibly other organics also being formed (e.g., Fang et al., 2021; Lal et al., 2000; Petrenko et al., 2013; van de Wal et al., 2007). ^{14}C production rates are highest near the surface, where neutron-induced spallation of ^{16}O is the main production mechanism. The neutron flux is attenuated rapidly with depth, however, and only affects the uppermost $\approx$ 20m of the firn (or uppermost $\approx$10 m of solid ice) (e.g., Lal et al., 1987). Below these depths, production of ^{14}C proceeds at lower rates and is dominated by negative muon capture as well as interactions with fast muons (Fig. 1b) (Petrenko et al., 2016; van der Kemp et al., 2002).
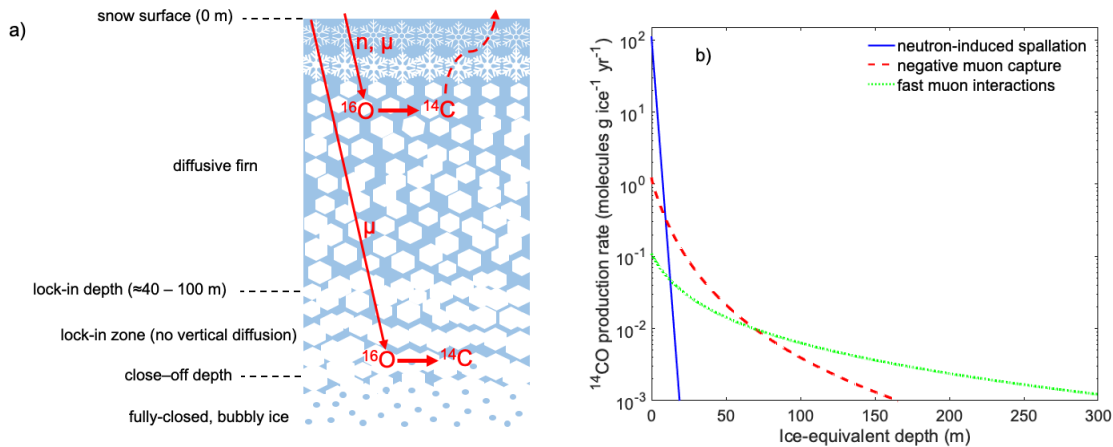
Figure 1: Introduction to production and loss of ^{14}C in firn and ice. a) Simplified schematic of the firn column, illustrating *in situ* cosmogenic production ^{14}C by neutrons (n) and muons (μ) and loss in the upper, diffusive part of

the firn as well as ^{14}C production by muons below the lock-in depth where all of the ^{14}C is retained. b) [14]CO production rates calculated as described in Section 2.2. Here $f_{\mu-}$ = 0.0667 and $f_{\mu f}$ = 0.0722, which are mid-range values from the range constrained by Hmiel et al. (2023).

100

The concentration of *in-situ* [14]C in glacial ice at accumulation sites is controlled by the ^{14}C production rates (site and depth-dependent), the snow accumulation rate and the retention of ^{14}C in the firn. Sites at higher altitudes have less atmospheric shielding from cosmic rays, resulting in higher ^{14}C production rates at the surface (e.g., Lifton et al., 2014). At sites with low accumulation rates, ice layers spend more time at relatively shallower depths, allowing

105   for more *in situ* [14]C to be produced. Further, prior work has shown that most of the *in situ* cosmogenic ^{14}C that is produced in the firn is rapidly lost to the atmosphere (de Jong et al., 2004; Hmiel et al., 2023; Petrenko et al., 2013). Because of this, the majority of the *in situ* cosmogenic ^{14}C in glacial ice is from production below the firn zone. Of the ^{14}C-containing gases in glacial ice, [14]CO has the highest ratio of *in situ* cosmogenic to trapped atmospheric [14]C. This is due to 1) atmospheric [14]CO concentrations being lower than those for [14]CO$_2$ or [14]CH$_4$ (mainly because global

110   mean mole fractions for CO ($\approx$80 nmol mol^{-1}) are much lower than those for CO$_2$ ($\approx$420 µmol mol^{-1}) and CH$_4$ ($\approx$1920 nmol mol^{-1}) (NOAA GML data viewer)) and 2) the relatively large fraction of *in situ* [14]C that forms CO in ice ($\approx$0.31; Dyonisius et al., 2023; Hmiel et al., 2023). This makes [14]CO the best species for investigating the *in situ* cosmogenic component of ^{14}C in ice.

In situ [14]CO in glacial ice is present at very low concentrations (a few molecules per gram ice is typical, see

115   Figures 2 and 3), making measurements very analytically challenging. Prior studies have either worked with relatively small (a few kg) ice samples available from a single shared ice core (e.g., van der Kemp et al., 2002), resulting in relatively large uncertainties, or required dedicated ice coring campaigns to obtain large ice amounts (100 kg or more) from multiple parallel ice cores for high-precision measurements (e.g, Dyonisius et al., 2023). Dry extraction of air from ice has been used for smaller ice samples (van der Kemp et al., 2002), and melt-extraction for large samples

120   (Dyonisius et al., 2023). CO in the extracted air is separated, combusted to CO$_2$, this CO$_2$ is subsequently converted to graphite and then the ^{14}C/^{13}C or ^{14}C/^{12}C ratio is measured via accelerator mass spectrometry. A detailed description of ice core [14]CO measurement methodology can be found in Dyonisius et al. (2023).

2.2 Production of [14]CO in glacial ice

Prior studies (Dyonisius et al., 2023; Hmiel et al., 2023) have presented detailed parameterizations of *in situ*

125   cosmogenic [14]CO production rates in glacial ice. This work uses the same parameterizations, which are described again here for the reader's convenience. [14]C production rate in ice via the neutron mechanism declines exponentially with depth, with [14]CO production rate calculated following Hmiel et al. (2023) as:

$$P_n^{CO}(h) = \Omega_{n}^{CO} \cdot F_n \cdot S_n \cdot Q_C \cdot P_{n,SLHL}^{Qtz}(0) \cdot e^{-h/\Lambda_n} \qquad (1)$$

In this equation, h is the mass-depth (in g cm^{-2}), Ω_{n}^{CO} is the fraction of total *in situ* [14]C that forms CO (we use 0.31,

130   following Hmiel et al. (2023)) and F_n is an adjustable dimensionless parameter that allows for tuning the neutron mechanism production rate within uncertainties (0.9 – 1.1 range). S_n is the site-specific dimensionless scaling factor

which describes the ratio of ^{14}C production rate at the site of interest to ^{14}C production rate at a sea-level high-latitude reference site; S_n is determined using the model of Lifton et al. (2014). Q_c is a factor that translates ^{14}C production rate from quartz to ice using the difference in oxygen atom density (atoms/g) between ice and quartz ($Q_c = 1.667$). $P_{n,SLHL}^{Qtz}(0)$ is the reference ^{14}C production rate at the surface via the neutron mechanism in quartz at a sea-level high-latitude site; we use a value of 12.76 atoms / g Qtz / yr from the CRONUS-Earth project, which is defined for 2001-2010 mean solar modulation and geomagnetic field conditions (Borchers et al., 2016). Λ_n is the absorption mean free path of neutrons in ice; we use a value of 150 g cm^{-2} (Lal et al., 1987; van de Wal et al., 2007).

For [14]CO production by the muon mechanisms, we use a model developed by Balco et al. (2008) ("Balco model"), which incorporates parameterizations of Heisinger et al. (2002a, 2002b). The ^{14}C production rate via negative muon capture in these parameterizations is calculated using:

$$P_{\mu-}(h) = R_{\mu-}(h) \cdot f_C \cdot f_D \cdot f^* \tag{2}$$

where $R_{\mu-}(h)$ is the stopping rate of negative muons (muons g^{-1} yr^{-1}) at mass-depth h, f_C is the chemical compound factor representing the probability that the stopped muon is captured by one of the target atoms, f_D is the probability that the negative muon does not decay in the K-shell before nuclear capture, and f^* is the effective probability for production of the cosmogenic nuclide of interest after μ^- capture by the target nucleus. For production of ^{14}C from [16]O in ice, $f_C = 1$, $f_D = 0.1828$ and $f^* = 0.137$ (Heisinger et al., 2002a).

The ^{14}C production rate via the fast muon mechanism is given by Heisinger et al. (2002b) as:

$$P_{\mu f}(h) = \sigma_0 \cdot \beta(h) \cdot \phi(h) \cdot \bar{E}(h)^\alpha \cdot N \tag{3}$$

where σ_0 is the reference nuclear reaction cross section at muon energy of 1 GeV (cm^2), $\phi(h)$ is the total muon flux at mass-depth h (muons cm^{-2} yr^{-1} sr^{-1}), $\bar{E}(h)$ is the mean muon energy at mass-depth h (GeV), α is a power factor that describes the energy dependence of the cross section (we use $\alpha=0.75$, consistent with Dyonisius et al., 2023 and Heisinger et al., 2002b), and N is the number of target nuclei per gram target mineral" (Hmiel et al., 2023). We use $\sigma_0 = 8.8$ μb = 8.8 x 10^{-30} cm^2 (Heisinger et al., 2002b) and N = (6.022 x 10^{23} atoms / mol) / (18.02 g / mol) for ice. $\beta(h)$ is a unitless depth dependence factor (≈0.9 at our depths of interest, with only a slight dependence on depth), given by Heisinger et al (2002b) as:

$$\beta(h) = \frac{\overline{E(h)^\alpha}}{\overline{E}(h)^\alpha} \tag{4}$$

Heisinger et al. (2002b) also provide an approximate function for $\beta(h)$, which is used in the Balco model and hence in our model:

$$\beta(h) = 0.846 - 0.015\ln(h+1) + 0.003139(\ln(h+1))^2 \tag{5}$$

The Balco model incorporates equations 2 and 3 and also provides the muon fluxes and energies as a function of mass-depth h for a given site, using site atmospheric pressure as input.

2.3 Constraints on *in situ* [14]CO production rates from measurements at Taylor Glacier, Antarctica

Recent studies at Taylor Glacier, Antarctica (an ice ablation site that exposes ancient ice at the surface) have provided measurements of ^{14}C in ice older than 50 ka (Dyonisius et al., 2023; Petrenko et al., 2016). In such ice, any ^{14}C from the snow accumulation site (from ^{14}C-containing atmospheric gases trapped into air bubbles or from *in situ*

cosmogenic production) has decayed away (^{14}C half-life is 5700 years), and the only measurable ^{14}C originates from relatively slow *in situ* cosmogenic production by muons as the glacier transports the ice at large depths and somewhat faster production as the ice gradually rises toward the surface via ablation. Due to the relatively fast ice ablation rate of ≈20 cm yr $^{-1}$, the ^{14}C contribution from the neutron production mechanism is negligible for ice deeper than 6 m. This presented an opportunity to use ^{14}CO measurements in Taylor Glacier to constrain the muogenic ^{14}CO production rates in ice in a natural setting.
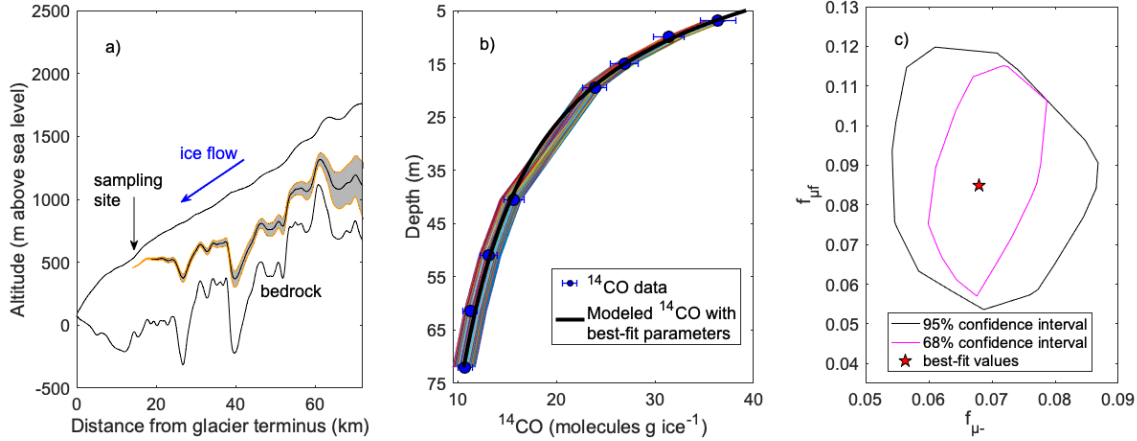
Figure 2. Overview of ^{14}CO results from Taylor Glacier. a) Ice parcel back-trajectories for the deepest (72 m) Taylor Glacier ^{14}CO sample. Solid black line shows the best-estimate flow trajectory and the shaded envelope represents the 68% CI. b) Comparison of Taylor Glacier ^{14}CO measurements with model predictions for accepted scenarios. c) accepted ranges of $f_{\mu-}$ and $f_{\mu f}$. Figures modified from Dyonisius et al. (2023).

Dyonisius et al. (2023) presented measurements of ^{14}CO in Taylor Glacier ice between the surface and 72 m depth. An ice flowline model for Taylor Glacier (Buizert et al., 2012b) was used to reconstruct the possible range of trajectories for the sampled ice parcels (Figure 2a). The Balco model was used to calculate ^{14}CO production via the muon mechanisms as ice parcels followed the trajectories. As prior work suggested that muogenic ^{14}C production rates from Heisinger et al. (2002a, 2002b) may be too high when applied to ice (Petrenko et al., 2016), Dyonisius et al. (2023) introduced production rate adjustment factors $f_{\mu-}$ and $f_{\mu f}$ into production rate equations as follows:

$$P_{\mu-}^{CO}(h) = f_{\mu-} \cdot P_{\mu-}^{Balco}(h, P) \tag{6}$$

$$P_{\mu f}^{CO}(h) = f_{\mu f} \cdot P_{\mu f}^{Balco}(h, P) \tag{7}$$

Here $P_{\mu}^{Balco}(h, P)$ is the total ^{14}C production rate (in atoms g^{-1} yr^{-1}) in the Balco model for the respective muon mechanism at mass-depth h and surface pressure P. $f_{\mu-}$ and $f_{\mu f}$ account for 1) the fraction of total ^{14}C that forms ^{14}CO (Ω^{CO}) and 2) adjustment factor for total ^{14}C production rate.

To define the best-estimate ^{14}CO production rate adjustment factors $f_{\mu-}$ and $f_{\mu f}$, Dyonisius et al. (2023) used a grid search approach, as follows. Using the best-estimate ice parcel back-trajectory (Fig. 2a), an expected ^{14}CO depth profile was calculated for each combination of $f_{\mu-}$ and $f_{\mu f}$ between 0 and 0.2 at 0.001 resolution. The model results were then compared to ^{14}CO measurements (Fig. 2b) with mean depths of 6.85 m or deeper (to avoid significant effects

from the neutron mechanism) and a χ^2 metric was used to determine the goodness of fit. To define the possible range of $f_{\mu-}$ and $f_{\mu f}$, Dyonisius et al. (2023) used a Monte Carlo approach, as follows. First, 10,000 possible ice back-trajectories were generated by perturbing ablation rates along the glacier according to their uncertainties (Fig. 2a). Next, a wide prior distribution for $f_{\mu-}$ and $f_{\mu f}$ was defined by starting with the best-estimate values and assuming a large and normally distributed 200% uncertainty in these values. 100,000 Monte Carlo iterations of the model were then run, with each iteration randomly selecting a back-trajectory scenario and a pair of $f_{\mu-}$ and $f_{\mu f}$ from the prior distribution described above. All pairs of $f_{\mu-}$ and $f_{\mu f}$ that yielded ^{14}CO depth profiles (Fig. 2b) that were within average measurement uncertainty (1σ or 2σ) from the best-fit solution were accepted (Fig. 2c).

2.3 Constraints on *in situ* ^{14}CO retention and leakage in firn and production in ice at Greenland Summit

In situ cosmogenic ^{14}C that is produced in the firn column above the lock-in depth can be lost to the atmosphere if it is able to leak out of the ice grains, resulting in low ^{14}C retention into ice below the firn zone (e.g., de Jong et al., 2004; Petrenko et al., 2013 and references therein). Hmiel et al. (2023) used Greenland Summit to conduct the most comprehensive study to date of *in situ* cosmogenic ^{14}C in the firn, with a focus on ^{14}CO. This study measured ^{14}CO in the ice grains in the firn matrix, in firn air, as well as in bubbly ice below the firn zone. Very large firn and ice samples (200 – 300 kg) were used for ^{14}CO analysis, to provide sufficiently large numbers of ^{14}C atoms for precise ^{14}C measurements. Figure 3a shows the ^{14}CO results for samples from the firn, firn-ice transition and bubbly ice below the firn zone. In the shallowest firn, ^{14}CO increases rapidly with depth owing mainly to production by the neutron mechanism, reaching a peak in the 10 – 20 m depth range. Beyond 20 m, ^{14}CO in the firn matrix declines gradually with depth in the diffusive part of the firn, reflecting leakage of *in situ* ^{14}C from the ice grains. ^{14}CO increases rapidly in the lock-in zone (≈70 – 80 m), reflecting addition of ^{14}CO from trapped air. Below the lock-in zone, ^{14}CO in the ice continues to increase gradually due to deeper production by the muon mechanisms.
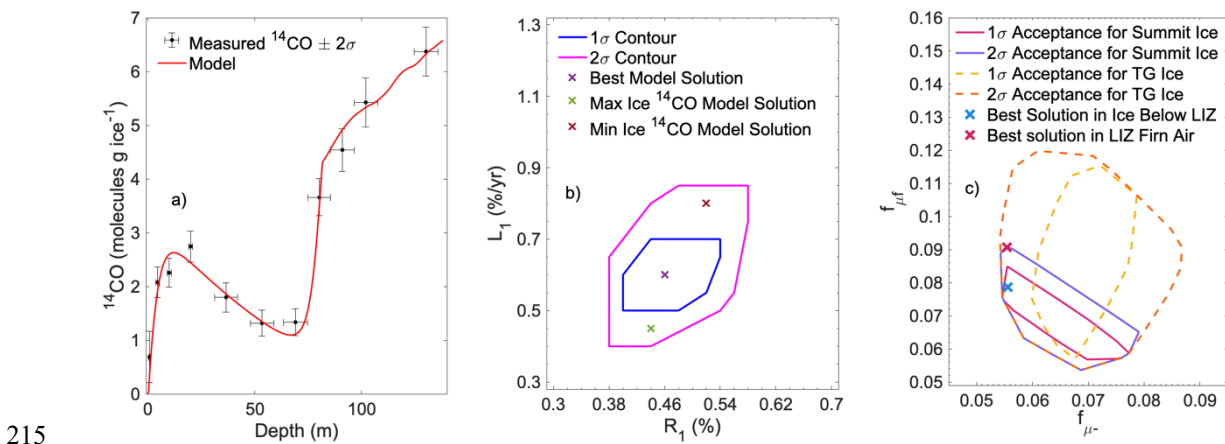
Figure 3. Overview of ^{14}CO results from Greenland Summit. a) Measured ^{14}CO content in ice grains and closed porosity along with a model fit. Horizontal error bars represent the depth range of firn and ice included in each sample. b) Contour plot of the accepted ranges of the R_1 (initial retention) and L_1 (slow leakage) parameters in firn, together

220   with the best-fit solution as well as solutions that result in maximum and minimum ^{14}CO content in ice below the firn zone. c) Contour plot of accepted ranges of f_{μ^-} and $f_{\mu f}$ from Taylor Glacier (dashed lines) and after further constraints from Summit measurements (solid lines).

225   To interpret the Greenland Summit ^{14}CO results, Hmiel et al. (2023) employed a firn gas transport model that can also characterize trapped air in ice below the firn zone (Buizert et al., 2012a). Production of *in situ* ^{14}C following the systematics described in section 2.2 and tracking of ^{14}C in ice grains and porosity was implemented into this model. With regard to ^{14}C loss from ice grains in the firn, it was found that the model-data agreement was best if two separate loss processes were parameterized in the model: a fast process, with a time scale <1 year and an additional slow process. This was described in the model using parameters R_1 and L_1. R_1 represents the fraction of *in situ* ^{14}C in the

230   ice grains that is initially retained. The fraction of *in situ* ^{14}C in ice grains that is lost rapidly, given by $1-R_1$, leaks out from the ice grains into the porosity at every model time step (0.5 year). L_1 represents the fraction of the initially retained ^{14}C that is lost more slowly from the ice grains over the course of 1 year. Hmiel et al. (2023) used a grid search approach to constrain the possible ranges of R_1 and L_1 at Summit (Fig. 3b), showing that >99% of *in situ* ^{14}C is lost rapidly from the ice grains, while the remaining $\approx$0.5% (R_1) of *in situ* ^{14}C continues to leak out slowly at a rate

235   of $\approx$0.6% per year (L_1). Hmiel et al. (2023) argued that the rapid loss is best explained by the process of gas diffusion through ice and suggested that the $\approx$0.5% of ^{14}C that is initially retained may be trapped in microbubbles or by impurities at dislocations or grain boundaries and is released via the process of recrystallization.

Greenland Summit ^{14}CO measurements in ice below the firn zone also provided an opportunity to test muon mechanism ^{14}CO production rate estimates from Taylor Glacier. For Greenland Summit ice samples, the contribution

240   from trapped atmospheric ^{14}CO is important ($\approx 25 - 40$ % of total) and uncertainties in the atmospheric ^{14}CO history interfere with precise constraints on f_{μ^-} and $f_{\mu f}$. Nevertheless, by trialing the Taylor Glacier sets of accepted on f_{μ^-} -- $f_{\mu f}$ pairs in combination with several possible atmospheric ^{14}CO histories, Hmiel et al. (2023) were able to further narrow the possible ranges of f_{μ^-} and $f_{\mu f}$ (Fig. 3c).

3 *In situ* cosmogenic ^{14}CO in ice cores as a possible proxy for GCR flux variability

245   **3.1 Basic concept for using ^{14}CO in ice cores as a GCR flux proxy**

As the Greenland Summit ^{14}CO results summarized above illustrate, the retention of *in situ* cosmogenic ^{14}CO through the upper firn column is very low. This means that the majority of *in situ* ^{14}CO found in ice below the firn zone originates from production by muons below the lock-in depth, where this ^{14}CO can no longer escape to the atmosphere. If the firn layer is sufficiently thick ($\approx 90 - 100$ m actual depth or ≈ 65 m ice equivalent depth), the muons

250   penetrating below the firn must have an energy of $\approx$15 GeV or greater at the surface (e.g., Rogers and Tristam, 1984). Such muons originate from primary GCR particles with energies of $\approx$100 GeV or greater (Gaisser et al., 2016). The part of the GCR flux possessing such energies is not affected appreciably by either the geomagnetic or the heliospheric magnetic fields. *In situ* cosmogenic ^{14}CO content in ice cores drilled at such sites thus can serve as a proxy of variations

in the primary GCR flux. This proxy is in principle free of the confounding effects discussed in the Introduction for
255   other past GCR flux indicators.

Several considerations are important for site selection in order to increase the likelihood of success with this proxy. First, the *in situ* ^{14}CO signal must be maximized to help with measurement sensitivity as well as to reduce interference from the trapped atmospheric ^{14}CO component. Second, the site must have a thick firn column. This is needed to ensure that ^{14}CO below the firn zone is produced only by muons originating from primary GCRs that are

260   sufficiently energetic to be unaffected by solar magnetic field variations. Third, there should be as little *in situ* ^{14}CO retained from the shallow firn as possible. ^{14}CO produced in the shallow firn originates from neutrons or lower-energy muons that are affected by solar magnetic field variations and may complicate interpretation. Fourth, ideally the site must be glaciologically stable over time in terms of accumulation rate and lock-in depth. Large temporal variations in these parameters may introduce additional uncertainties in the interpretation, as they affect the predicted *in situ* ^{14}CO

265   content.

Considering the above, ice dome sites in the East Antarctic interior are most promising for attempting to examine past GCR flux variability using ^{14}CO in ice cores. Low accumulation rates at such sites maximize cosmogenic exposure times and thereby the *in situ* ^{14}CO signal. These sites also tend to have sufficiently thick firn columns (e.g., Buizert, 2013). The combination of low accumulation rate and thick firn column results in very long ice layer transit

270   times through the firn, maximizing the chance that *in situ* ^{14}CO produced by neutrons and low-energy muons in the shallow firn would be lost. Finally, dome sites are free of complications of upstream ice advection and ice core water stable isotope records suggest that interior East Antarctic climate has been stable over the last few thousand years (recent decades excepted) (e.g., Jouzel et al., 2001).

3.2 Using model predictions to explore Dome C, Antarctica as a test case for the ^{14}CO GCR flux proxy

275   Dome C, Antarctica is a site that meets the criteria needed for the ^{14}CO GCR flux proxy to be viable. It has been glaciologically very well characterized as a result of previous ice coring campaigns (e.g., EPICA community members, 2004, Nature) and has well-established logistical access owing to the permanent Concordia station. Further, a scientific ice drilling expedition is planned for the near future to Dome C for the purpose of ^{14}CO reconstruction at this site. We therefore use Dome C as an example site for more detailed model-based exploration of the ^{14}CO past

280   GCR flux proxy. We first applied the full firn-ice model mentioned above (Buizert et al., 2012a; Hmiel et al., 2023) to explore the (unwanted) contribution of ^{14}CO originating from production in the shallow firn as well as trapped atmospheric ^{14}CO to the overall ^{14}CO signal in ice below the firn zone. In the model, we used an accumulation rate of 3.2 cm ice equivalent yr^{-1}, firn density profile from the FIRETRACC project (EU FIRETRACC Campaign participants, 2006), and tuned the firn gas diffusivity profile based on a combination of available CO_2, CH_4, CFC-11,

285   CFC-12, CFC-113, CH_3CCl_3, SF_6 and $\delta^{15}N$ of N_2 measurements (EU FIRETRACC Campaign participants, 2006) . For parameters relevant to *in situ* ^{14}CO, we used $F_n = 1.03$, $R_1 = 0.44\%$ and $L_1 = 0.45\%$ yr^{-1} (see Section 2), which was the combination of values at Greenland Summit that maximized the amount of *in situ* ^{14}CO produced in the shallow firn that is retained into ice below the firn zone (Fig. 3b). For muogenic ^{14}CO production, we used $f_{\mu-} = 0.065$ and $f_{\mu f} = 0.07$, which are mid-range choices from the possible range of values that were consistent with both Taylor

290 Glacier and Summit measurements (Fig. 3c). We used a constant concentration of 12 molecules / cm^3 STP for the atmospheric ^{14}CO history, which is the average of the longest available Antarctic atmospheric ^{14}CO record (Manning et al., 2005).

Figure 4a shows model-calculated ^{14}CO content that represents the sum of ^{14}CO in ice grains and closed porosity (this is what measurements done with a melt-extraction approach would provide). The solid black line shows
295 results with both *in situ* and atmospheric ^{14}CO included in the model. There is a sharp ^{14}CO peak at ≈ 9 m depth that represents ^{14}CO in ice grains and is driven by intense ^{14}CO production by the neutron mechanism in near-surface firn. ^{14}CO then declines to near zero by ≈ 70 m due to slow leakage out of ice grains (controlled by the L_1 parameter in the model). At depths >80 m, the amount of closed porosity starts to increase, and this increases ^{14}CO by trapping of ^{14}CO from open porosity and by allowing more *in situ* ^{14}CO to be retained. This process further accelerates at ≈ 95 m, which
300 is the lock-in depth at Dome C. Below the close-off depth at Dome C (≈ 100 m), ^{14}CO content continues to increase due to production by muons, rising to 8.5 ^{14}CO molecules / g ice at the deepest modeled level (110 m).

The dashed blue line shows the expected contribution to total ^{14}CO from *in situ* ^{14}CO originating only from the shallower part of the firn. This was assessed by setting the atmospheric ^{14}CO history to zero and setting *in situ* production rates to zero for depths > 54 m ice equivalent. This contribution is < 0.5 ^{14}CO molecules / g ice and is due
305 to ^{14}CO that leaks out from ice grains in the shallow firn, diffuses into the deep firn and is subsequently trapped in air bubbles. The contribution from trapped atmospheric ^{14}CO (dotted pink line; assessed by turning off *in situ* production in the model) is < 1.2 ^{14}CO molecules / g ice. ^{14}CO originating from the sum of shallow *in situ* cosmogenic production and air trapping (solid red line) is < 1.6 ^{14}CO molecules / g ice at all depths below the firn zone.

We next examined the *in situ* cosmogenic ^{14}CO component at Dome C arising from production by deep-
310 penetrating muons, as well as its suitability for detecting changes in the past GCR flux. As this approach involved generating thousands of simulated data sets (see Section 3.3 below), we created a simple and computationally efficient ice-only model of *in situ* cosmogenic ^{14}CO for this test of proxy concept. This ice-only model has its starting (shallowest) depth in the lock-in zone and assumes an initial ^{14}CO content of zero. ^{14}CO production in the model is implemented following parameterizations described above in Section 2, with production rates within the range
315 constrained by Taylor Glacier and Summit results. The model assumes that all of the *in situ* ^{14}CO is retained and also includes ^{14}C radioactive decay. The model defines annual ice layers and shifts these layers downward on an annual basis following the ice layer age scale for Dome C from Buizert et al. (2018). For the purposes of this test of proxy concept, we set the deepest model depth at 300 m, as this is the practical limit for light ice coring projects that do not use drilling fluid and the deepest depth in the planned fieldwork. The exact starting depth of the model was chosen by
320 comparing predictions of this ice-only model with predictions from the full firn-ice model in the 100 – 110 m depth range (below close-off depth) when using the same muogenic ^{14}CO production rates and setting atmospheric ^{14}CO history to zero; using 96.5 m for the starting depth yields the best match.
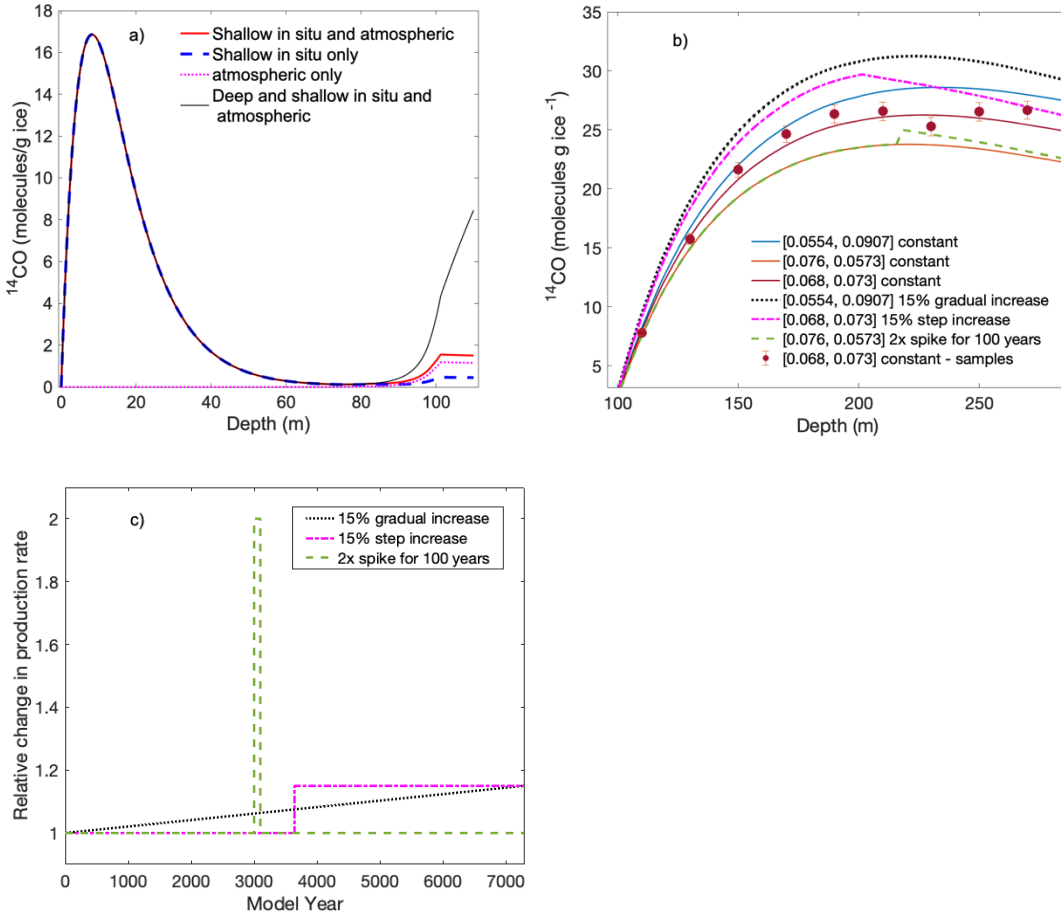
Figure 4. Predicted ^{14}CO content at Dome C. a) Predicted ^{14}CO content in ice grains + closed porosity (bubbles) from the full firn-ice model considering all ^{14}CO contributions as well as contributions from individual ^{14}CO components. b) Predicted *in situ* ^{14}CO content in ice below the firn zone from a simple ice-only model. The legend indicates the combination of [$f_{\mu-}$, $f_{\mu f}$] values (see Section 2) used in each model run, as well as whether the production rate was assumed to be constant (solid lines) or variable (dashed and dotted lines) in time. Markers illustrate what sample measurements might look like assuming 20 m depth averaging and a random 1σ measurement error of 3%. c) Time-variable production rate scenarios used to generate the corresponding depth-^{14}CO profiles in panel b).

Figure 4b illustrates predictions of the simple ice model for a few scenarios involving different combinations of $f_{\mu-}$ and $f_{\mu f}$ as well as different production rate histories (representing past GCR flux variations), and Figure 4c illustrates the time-variable production rate scenarios reflected in Figure 4b. Because *in situ* cosmogenic ^{14}CO production takes place at the full range of modeled depths (with production rate declining with depth as illustrated in Figure 1b), the ^{14}CO values at each depth represent a time integral of production rate minus the ^{14}C decay rate. As expected, ^{14}CO content increases most rapidly at the shallowest depths, followed by a broad peak in the 200 – 250 m depth range. For deeper ice, the rate of ^{14}CO removal via radioactive decay exceeds the rate of production by muons, and ^{14}CO values gradually decline. The modeled ice layers at Dome C span an age range of 7283 years, meaning that

an ice core ^{14}CO record reaching 300 m depth could offer information about past GCR flux variations for most of the Holocene.

Predicted ^{14}CO content originating from deep-penetrating muons is between 20 and 30 molecules g ice^{-1} for most of the modeled depth range. This means that the ^{14}CO contribution arising from trapped atmospheric ^{14}CO and ^{14}CO production in shallow firn (<1.6 molecules g ice^{-1}; Fig. 4a) would contribute <8% of total ^{14}CO and is unlikely to interfere with ^{14}CO signal interpretation. We note that there were 3 prior ^{14}CO measurements that were made on the Dome C ice core in the depth range we are considering (de Jong et al., 2004). Those measurements were made on much smaller (1 – 2 kg) samples than Taylor Glacier and Summit measurements, and thus were associated with very large uncertainties (50 – 100%, considering only uncertainty reported for ^{14}C activities). That said, de Jong et al. (2004) reported ^{14}CO values in the 15 – 30 molecules g ice^{-1} range for these 3 samples and concluded that there was no detectable *in situ* ^{14}C retention from the firn, consistent with our model predictions.

Figure 4b illustrates that the absolute ^{14}CO content in the ice as well as the depth of the ^{14}CO peak depend on the balance of production rates from the negative muon capture and fast muon mechanisms (solid lines); this is controlled by $f_{\mu-}$ and $f_{\mu f}$ parameters in the model. In the modeled depth range, the fast muon mechanism is relatively more important (Fig. 1b), so maximizing $f_{\mu f}$ at the expense of $f_{\mu-}$ (within the range on Fig. 3c) increases total ^{14}CO and shifts the peak slightly deeper. Despite these differences, the shape of the depth – ^{14}CO curves remains largely similar. Figure 4b also illustrates a few scenarios where the production rates (controlled by GCR flux) vary in time (dashed and dotted lines). For time-variable production rates for the purpose of this illustration (Fig. 4c), we trialed 1) a scenario where production by each muon mechanism increases at a linear rate over the entire duration of the model run, reaching 15% higher rates by the end of the run (black dotted line); 2) a scenario where there is a 15% step increase in production rates halfway through the model run (pink dash-dot line) and 3) a scenario where there is a 2x transient step increase in production rates that takes places between 3000 and 3100 years in the model run (green dashed line). As can be seen, all of these types of variations produce depth – ^{14}CO profiles that are distinct in their shape from the constant production rate scenarios.

3.3 Analysis of sensitivity of ice core ^{14}CO measurements at Dome C to variations in past GCR flux

We compare several time-varying scenarios to the baseline model of a constant GCR flux with muonic production rates ($f_{\mu-}$, $f_{\mu f}$) that are consistent with ice core ^{14}CO measurements in both Dyonisius et al. (2023) and Hmiel et al. (2023). As shown in Figure 4b, deviations from the baseline model can be produced by temporal variations in the GCR flux. However, in the presence of a steady-state flux, uncertainties in the muonic production rates also create deviations from the baseline model. While the normalization of the depth-^{14}CO profile is affected by both the temporal variations in the GCR flux and the production rates, the shape of the profile is more sensitive to temporal variations in the flux. Therefore, we develop an analysis that is sensitive to the shape of the ^{14}CO profile as a function of depth.

To discriminate the steady-state GCR scenario H_0 from the time-varying scenario H_1, we construct a test statistic using a Bayes factor (Jeffreys 1998, Kass and Raftery 1995):

$$B_{01} = \frac{P(\vec{c}|H_0)}{P(\vec{c}|H_1)} = \frac{\int d\vec{\theta}_0 \, P(\vec{c}|\vec{\theta}_0, H_0) P(\vec{\theta}_0|H_0)}{\int d\vec{\theta}_1 \, P(\vec{c}|\vec{\theta}_1, H_1) P(\vec{\theta}_1|H_1)} \tag{8}$$

In this expression, $\vec{c} = \{c(h_j)\}$ is a ^{14}CO profile measured as a function of discrete depths $h_j = \{h_1, \dots, h_N\}$. The Bayes factor computes the ratio of the marginal probabilities of measuring ^{14}CO profile $\vec{c}$ given the steady-state and time-varying scenarios H_0 and H_1. If the data provide greater evidence for the steady-state hypothesis H_0, $B_{01} > 1$, and if the time-varying hypothesis is supported, $B_{01} < 1$.

During the calculation of B_{01}, each marginal probability, $P(\vec{c}|H_i)$, can be factorized into two terms: a conditional probability $P(\vec{c}|\vec{\theta}_i, H_i)$, where $\vec{\theta}_i$ lists the free parameters of GCR flux model H_i; and a "prior" probability distribution $P(\vec{\theta}_i|H_i)$. To complete the calculation, we integrate over the possible values of the parameters $\vec{\theta}_i$ in each model H_i. The prior probabilities specify the allowed ranges of parameters $\vec{\theta}_i$ in model H_i and allow us to weight the calculation toward more probable values of the model parameters. Note that we are free to choose the functional form of the prior distributions using theoretical considerations, past measurements, or even our subjective degree of belief in the most likely values of the parameters of a given model. In this work, we use non-informative (or "flat") prior distributions that do not favor any particular values of the model parameters, beyond restricting their ranges to physically motivated regions.

In the sensitivity calculation, the muonic production rates ($f_{\mu\text{-}}$, $f_{\mu f}$) are nuisance parameters folded into both $\vec{\theta}_0$ and $\vec{\theta}_1$. Using the confidence intervals on ($f_{\mu\text{-}}$, $f_{\mu f}$) from Dyonisius et al. (2023) and Hmiel et al. (2023), we can factorize the prior probability $P(\vec{\theta}_i|H_i)$ for model i into a joint prior $P(f_{\mu\text{-}}, f_{\mu f}|H_i)$ and a set of independent priors dependent on the parameters of the model. For example, the joint prior $P(f_{\mu\text{-}}, f_{\mu f}|H_i)$ is given by the "2σ acceptance from Summit ice" contour in Figure 3c. If we wish to test a cosmic ray model H_1 with a flux that varies linearly in time, the model includes an additional free parameter a representing the rate of change of the flux as a function of time. In the calculation of the Bayes factor, the prior distribution of a is a uniform probability density function

$$P(a|H_1) = \begin{cases} \frac{1}{a_{\max} - a_{\min}}, & a \in [a_{\min}, a_{\max}] \\ 0, & \text{otherwise} \end{cases} \tag{9}$$

Here $a_{\min}$ and $a_{\max}$ represent the allowed range of values we consider for the rate of change of the flux. We use a uniform distribution for $P(a|H_1)$ because it is unbiased, giving equal weight to all values of a between $a_{\min}$ and $a_{\max}$.

Our calculation assumes the ice core ^{14}CO measurements are depth-averaged over 20 m, and each measurement has independent Gaussian uncertainties with relative sizes of 2% at 1σ. The 20 m depth averaging is assumed because this would provide the needed amount of ice for high precision ^{14}CO measurements (≈ 140 kg with a 10 cm-diameter ice core). Recent improvements in analytical techniques for ice core and atmospheric ^{14}CO measurements (Petrenko et al., 2023; Petrenko et al., 2021) make 2% uncertainties achievable, although for completeness we also repeat the calculations assuming 3% 1σ uncertainties. The conditional probability of observing a ^{14}CO profile $\vec{c}$ given GCR model H_i with parameters $\vec{\theta}_i$ is

$$P(\vec{c}|\vec{\theta}_i, H_i) = \prod_{j=1}^{N} \frac{1}{\sqrt{2\pi}\sigma_j} \exp\left\{-\frac{1}{2}\left(\frac{c_j - \hat{c}(h_j|\vec{\theta}_i, H_i)}{\sigma_j}\right)^2\right\} \tag{10}$$

Here $\hat{c}(h_j|\vec{\theta}_i, H_i)$ is the expected ^{14}CO profile at depth h_j, which we compute using the model, while $c_j = c(h_j)$ is the observed ^{14}CO concentration at depth h_j. Since the measurement uncertainties are independent and Gaussian, the probability is the product of N independent Gaussian probability density functions over the N measurements in the depth profile. Multiplying this probability by the prior distributions of the nuisance parameters $(f_{\mu\text{-}}, f_{\mu f})$ and the allowed prior ranges of the model parameters (such as the slope of the linear change in the GCR flux) allows us to account for both systematic and statistical uncertainties in the measurement.

We calculate our sensitivity to a given GCR scenario as follows:

1. We produce 5×10^6 random realizations of the ^{14}CO profile at Dome C, assuming a constant production rate but accounting for the systematic uncertainties in $(f_{\mu\text{-}}, f_{\mu f})$. The profiles are generated with depth averaging of 20 m, and relative measurement uncertainties of $\sigma_j/c_j = 2\%$ and 3% are both investigated.

2. For each time-varying model under consideration, we compute a distribution of Bayes factors B_{01} using the random constant-flux data sets. This provides us with a distribution of the Bayes factor when the null constant-flux hypothesis H_0 is true.

3. We next produce a large set of independent ^{14}CO profiles assuming the alternative time-varying hypothesis H_1 is true and compute the Bayes factor B_{01}^* for each simulated data set. We expect that B_{01}^* will be much smaller than B_{01}, on average, since $P(\vec{c}|H_1) > P(\vec{c}|H_0)$ when the alternative hypothesis H_1 is true.

4. For each B_{01}^*, we compute the tail probability, or p-value, that gives the probability a constant flux model will produce a Bayes factor smaller than the time-varying model purely by a chance statistical fluctuation:

$$p = P(B_{01} < B_{01}^*|H_0) \tag{11}$$

The reported sensitivity of a given model is the value of the model parameter(s) in which at least 50% of simulated data sets yield $p < 10^{-3}$ (3σ evidence against the steady-state model). We also report the value of the model parameter(s) yielding $p < 3\times10^{-7}$, corresponding to a 5σ discovery of a time-varying flux. This "calibration" of the Bayes factor accounts for the chance probability that a steady-state flux could produce a false positive report of a time-varying flux.

We investigated scenarios involving 1) a linear GCR flux increase over the entire duration of the record, 2) a step-like increase at approximately the mid-point of the record and 3) a brief (100 year) burst in the GCR flux. The results are reported in Table 1. For a scenario H_1 where the GCR flux increases linearly with time, and assuming 2% (3%) relative uncertainties in the measured ^{14}CO profile, a flux increase $a = 4\%$ (5%) over 7 ka is required to produce a 3σ evidence of a non-steady flux in at least 50% of simulated data sets. For a 5σ detection, the rate of change of the flux must be at least $a = 6\%$ (7%). We also investigated and found similar sensitivities for a scenario involving a step-like increase in the GCR flux at 3.5 ka. Much larger GCR flux changes are required for detection in the impulsive burst scenario: 250% (350%) for 3σ evidence. This is likely due to the large amount of temporal averaging (≈700 yr) that is imposed by the 20 m depth averaging for the measurements and the fact that the ^{14}CO content at each depth level represents a time integral of production rates. We further note that improving the relative uncertainty in the ^{14}CO measurement from 3% to 2% has a minor effect on the sensitivity to linear and step-like increases in the GCR flux, but the change in sensitivity to burst-like increases in the flux is substantial.

Difference from Baseline Model	Sensitivity	
	3σ (>50% of trials)	5σ (>50% of trials)
Linear increase over 7 ka	4% (5%)	6% (7%)
Step-like increase at 3.5 ka	4% (5%)	6% (7%)
Impulsive increase lasting 100 yr at 3.5 ka	250% (350%)	350% (460%)

Table 1. Simulated sensitivity to temporal changes in the GCR flux. We report the magnitude of GCR flux changes
in time-varying models required to produce a 3σ or 5σ detection in at least 50% of simulated data sets, assuming 2%
(3%) relative uncertainties in the ^{14}CO measurements. For example, to produce a 3σ detection of a linearly increasing
or decreasing GCR flux, the rate of change of the flux must be at least 4% (5%) over 7 ka.

4 Conclusions

^{14}CO in ice cores at low-accumulation sites such as Dome C, Antarctica has good potential to provide a test
of the assumption of GCR flux constancy over the Holocene and to serve as a proxy for past variations in the GCR
flux on timescales of a few thousand years. ^{14}CO measurements in the proposed approach would be most sensitive to
gradual linear or step-like changes in the GCR flux, in principle allowing to test the assumption of GCR flux constancy
to 5% or better. This would represent a large improvement over the ≈30% uncertainty associated with constraints from
meteorite measurements. Because our approach involves a large amount of temporal averaging, sensitivity to short-
lived GCR bursts is much worse. However, such bursts (if present) would have been captured by high-resolution
records of other cosmogenic nuclides such as ice core ^{10}Be and tree-ring ^{14}C.

We note that cosmogenic nuclides produced in the atmosphere such as ^{10}Be are primarily sensitive to the
GCR flux below 10 GeV, while the ^{14}CO proxy discussed here is sensitive to the flux above 100 GeV. The extent to
which temporal variations in the GCR flux above 100 GeV would produce proportional changes below 10 GeV, while
beyond the scope of this paper, is an interesting question to consider, as the answer depends on the origin of the
temporal variations. Since the diffusion length of cosmic rays increases with energy, it is reasonable to expect that a
constant GCR flux at high energy is likely to imply a constant GCR flux below 10 GeV, while a time-varying flux
above 100 GeV could still be consistent with a constant flux at or below 10 GeV.

For most precise results, the ^{14}CO proxy approach requires an ice dome site that is glaciologically stable
(accumulation rate, lock-in depth) over the duration of the GCR flux reconstruction. Although our work indicates that
the ^{14}CO GCR flux proxy is likely to provide useful results for most of the Holocene, we expect that GCR flux
reconstructions beyond the Holocene with this approach would be more challenging, owing to 1) the need for drilling
fluid to obtain ice below ≈ 300m, which would greatly increase logistical requirements and introduce added challenges
of CO contamination from the drilling fluid, 2) glaciological changes beyond the Holocene and 3) reduced ^{14}CO signal
at greater depths due to ^{14}C radioactive decay.

Code availability

Code for the firn and ice models as well as for the statistical analysis used in this study is available from

475 https://github.com/14CO/Dome-C-Sensitivity

Data availability

The simulated data sets created as part of the statistical analysis in this study are available from

https://github.com/14CO/Dome-C-Sensitivity.

480

Author Contribution

VVP and SB developed the ^{14}CO GCR flux proxy concept. VVP wrote the code for the simple ice model and performed firn and ice model simulations. SB developed the approach, wrote the code for and performed statistical analyses. CB provided firn model tuning and ice layer age scale for Dome C. VVP and SB wrote the manuscript, with

485 input from all other authors.

Competing Interests

The authors declare that they have no conflict of interest.

490 **Acknowledgements**

This work was funded by the University of Rochester Bridging Fellowship (to VVP) and US NSF Award OPP-2146131 (to VVP and SB). We thank I. Usoskin, R. Muscheler, G. Balco, J. Stone and N. Lifton for helpful discussions.

495

References

Abeysekara, A. U. and Alfaro, R. and Alvarez, C. et al. [HAWC Collaboration] and Aartsen, M. G. and Ackermann, M. and Adams, J. et al. [IceCube Collaboration]: All-sky Measurement of the Anisotropy of Cosmic Rays at 10 TeV and Mapping of the Local Interstellar Magnetic Field, Astrophys. J., 871:96, 2019.

Adolphi, F., Muscheler, R., Svensson, A., Aldahan, A., Possnert, G., Beer, J., Sjolte, J., Bjorck, S., Matthes, K., and Thieblemont, R.: Persistent link between solar activity and Greenland climate during the Last Glacial Maximum, Nature Geosci., 7, 662-666, 2014.

Ahlers, M. and Mertsch, P.: Small-Scale Anisotropies of Cosmic Rays from Relative Diffusion, Astrophys. J. Lett., 815:L2, 2015.

Balco, G.: Contributions and unrealized potential contributions of cosmogenic-nuclide exposure dating to glacier chronology, 1990-2010, Quatern. Sci. Rev., 30, 3-27, 2011.

Balco, G.: Glacier Change and Paleoclimate Applications of Cosmogenic-Nuclide Exposure Dating, Ann. Rev. Earth Planet. Sci., 48, 21-48, 2020.

Balco, G., Stone, J. O., Lifton, N. A., and Dunai, T. J.: A complete and easily accessible means of calculating surface exposure ages or erosion rates from Be-10 and Al-26 measurements, Quatern. Geochronol., 3, 174-195, 2008.

Bard, E., Raisbeck, G., Yiou, F., and Jouzel, J.: Solar irradiance during the last 1200 years based on cosmogenic nuclides, Tellus B, 52, 985-992, 2000.

Blasi, P. and Amato, E.: Diffusive propagation of cosmic rays from supernova remnants in the Galaxy. II: anisotropy, J. Cosmol. Astropart. Phys., Artn 011, 2012.

Borchers, B., Marrero, S., Balco, G., Caffee, M., Goehring, B., Lifton, N., Nishiizumi, K., Phillips, F., Schaefer, J., and Stone, J.: Geological calibration of spallation production rates in the CRONUS-Earth project, Quatern. Geochronol., 31, 188-198, 2016.

Buizert, C.: Studies of Firn Air. In: The Encyclopedia of Quaternary Science, Elias, S. A. (Ed.), Elsevier, Amsterdam, 2013.

Buizert, C., Martinerie, P., Petrenko, V. V., Severinghaus, J. P., Trudinger, C. M., Witrant, E., Rosen, J. L., Orsi, A. J., Rubino, M., Etheridge, D. M., Steele, L. P., Hogan, C., Laube, J. C., Sturges, W. T., Levchenko, V. A., Smith, A. M., Levin, I., Conway, T. J., Dlugokencky, E. J., Lang, P. M., Kawamura, K., Jenk, T. M., White, J. W. C., Sowers, T., Schwander, J., and Blunier, T.: Gas transport in firn: multiple-tracer characterisation and model intercomparison for NEEM, Northern Greenland, Atmos. Chem. Phys., 12, 4259-4277, 2012a.

Buizert, C., Petrenko, V. V., Kavanaugh, J. L., Cuffey, K. M., Lifton, N. A., Brook, E. J., and Severinghaus, J. P.: In situ cosmogenic radiocarbon production and 2-D ice flow line modeling for an Antarctic blue ice area, J. Geophys. Res., 117, 2012b.

Buizert, C., Sigl, M., Severi, M., Markle, B. R., Wettstein, J. J., McConnell, J. R., Pedro, J. B., Sodemann, H., Goto-Azuma, K., Kawamura, K., Fujita, S., Motoyama, H., Hirabayashi, M., Uemura, R., Stenni, B., Parrenin, F., He, F., Fudge, T. J., and Steig, E. J.: Abrupt ice-age shifts in southern westerly winds and Antarctic climate forced from the north, Nature, 563, 681-685, 2018.

de Jong, A. F. M., Alderliesten, C., van der Borg, K., van der Veen, C., and van De Wal, R. S. W.: Radiocarbon analysis of the EPICA Dome C ice core: no in situ C-14 from the firn observed, Nucl. Instrum. Methods B, 223-24, 516-520, 2004.

Dyonisius, M. N., Petrenko, V. V., Smith, A. M., Hmiel, B., Neff, P. D., Yang, B., Hua, Q., Schmitt, J., Shackleton, S. A., Buizert, C., Place, P. F., Menking, J. A., Beaudette, R., Harth, C., Kalk, M., Roop, H. A., Bereiter, B., Armanetti, C., Vimont, I., Michel, S. E., Brook, E. J., Severinghaus, J. P., Weiss, R. F., and McConnell, J. R.: Using ice core measurements from Taylor Glacier, Antarctica, to calibrate in situ cosmogenic C-14 production rates by muons, Cryosphere, 17, 843-863, 2023.

EPICA Community Members: Eight glacial cycles from an Antarctic ice core, Nature, 429, 623 – 628, 2004.

Erlykin, A. D. and Wolfendale, A. W.: The anisotropy of galactic cosmic rays as a product of stochastic supernova explosions, Astropart. Phys., 25, 183-194, 2006.

EU FIRETRACC Campaign participants; Atlas, E. B., J.-M.; Brenninkmeijer, C.; Mulvaney, R.; Schwander, J.; Sturges, W.T.; Penkett, M.; Penkett, S.A.; Chappellaz, J.; Jouzel, J. : Firn Record of Trace Gases Relevant to Atmospheric Chemical Change over 100 yrs (FIRETRACC/100). NCAS British Atmospheric Data Centre, 2006.

Fang, L., Jenk, T. M., Singer, T., Hou, S. G., and Schwikowski, M.: Radiocarbon dating of alpine ice cores with the dissolved organic carbon (DOC) fraction, Cryosphere, 15, 1537-1550, 2021.

Field, C. V., Schmidt, G. A., Koch, D., and Salyk, C.: Modeling production and climate-related impacts on Be-10 concentration in ice cores, J. Geophys. Res., 111, D15107, 2006.

Gaisser, T. K., Engel, A., and Resconi, E.: Cosmic Rays and Particle Physics, Cambridge University Press, 2016.

Gosse, J. C. and Phillips, F. M.: Terrestrial in situ cosmogenic nuclides: theory and application, Quatern. Sci. Rev., 20, 1475-1560, 2001.

Heisinger, B., Lal, D., Jull, A. J. T., Kubik, P., Ivy-Ochs, S., Knie, K., and Nolte, E.: Production of selected cosmogenic radionuclides by muons: 2. Capture of negative muons, Earth Planet. Sci. Lett., 200, 357-369, 2002a.

Heisinger, B., Lal, D., Jull, A. J. T., Kubik, P., Ivy-Ochs, S., Neumaier, S., Knie, K., Lazarev, V., and Nolte, E.: Production of selected cosmogenic radionuclides by muons 1. Fast muons, Earth Planet. Sci. Lett., 200, 345-355, 2002b.

Hmiel, B., Petrenko, V. V., Buizert, C., Smith, A. M., Dyonisius, M. N., Place, P., Yang, B., Hua, Q., Beaudette, R., Severinghaus, J. P., Harth, C., Weiss, R. F., Davidge, L., Diaz, M., Pacicco, M., Menking, J. A., Kalk, M., Faïn, X., Adolph, A., Vimont, I., and Murray, L. T.: Characterization of in situ cosmogenic 14CO production, retention and loss in firn and shallow ice at Summit, Greenland, Cryosphere Discuss., 2023.

Jeffreys, H.: Theory of Probability, Oxford University Press, Oxford, U.K., 1998.

Jouzel, J., Masson, V., Cattani, O., Falourd, S., Stievenard, M., Stenni, B., Longinelli, A., Johnsen, S. J., Steffenssen, J. P., Petit, J. R., Schwander, J., Souchez, R., and Barkov, N. I.: A new 27 ky high resolution East Antarctic climate record, Geophys. Res. Lett., 28, 3199-3202, 2001.

Kachelriess, M., Neronov, A., and Semikoz, D. V.: Signatures of a Two Million Year Old Supernova in the Spectra of Cosmic Ray Protons, Antiprotons, and Positrons, Phys. Rev. Lett., 115, 2015.

Kass, R. E. and Raftery, A. E.: Bayes Factors, J. Am. Stat. Assoc., 90, 773-795, 1995.

570   Knudsen, M. F., Riisager, P., Donadini, F., Snowball, I., Muscheler, R., Korhonen, K., and Pesonen, L. J.: Variations in the geomagnetic dipole moment during the Holocene and the past 50 kyr, Earth Planet. Sci. Lett., 272, 319-329, 2008.

Knudsen, M. F., Riisager, P., Jacobsen, B. H., Muscheler, R., Snowball, I., and Seidenkrantz, M. S.: Taking the pulse of the Sun during the Holocene by joint analysis of (14)C and (10)Be, Geophys. Res. Lett., 36, 2009.

575   Koll, D., Korschinek, G., Faestermann, T., Gomez-Guzman, J. M., Kipfstuhl, S., Merchel, S., and Welch, J. M.: Interstellar Fe-60 in Antarctica, Phys. Rev. Lett., 123, 2019.

Lal, D., Jull, A. J. T., Burr, G. S., and Donahue, D. J.: Measurements of in situ C-14 concentrations in Greenland Ice Sheet Project 2 ice covering a 17-kyr time span: Implications to ice flow dynamics, J. Geophys. Res., 102, 26505-26510, 1997.

580   Lal, D., Jull, A. J. T., Burr, G. S., and Donahue, D. J.: On the characteristics of cosmogenic in situ C-14 in some GISP2 Holocene and late glacial ice samples, Nucl. Instrum. Methods B, 623-631, 2000.

Lal, D., Nishiizumi, K., and Arnold, J. R.: Insitu Cosmogenic H-3, C-14, and Be-10 for Determining the Net Accumulation and Ablation Rates of Ice Sheets, J. Geophys. Res., 92, 4947-4952, 1987.

Lifton, N., Sato, T., and Dunai, T. J.: Scaling in situ cosmogenic nuclide production rates using analytical
585   approximations to atmospheric cosmic-ray fluxes, Earth Planet. Sci. Lett., 386, 149-160, 2014.

Manning, M. R., Lowe, D. C., Moss, R. C., Bodeker, G. E., and Allan, W.: Short-term variations in the oxidizing power of the atmosphere, Nature, 436, 1001-1004, 2005.

Melott, A. L., Thomas, B. C., Kachelriess, M., Semikoz, D. V., and Overholt, A. C.: A Supernova at 50 pc: Effects on the Earth's Atmosphere and Biota, Astrophys. J., 840, 2017.

590   Mertsch, P. and Funk, S.: Solution to the Cosmic Ray Anisotropy Problem, Phys. Rev. Lett. 114, 021101, 2015.

Muscheler, R.: 10Be and Cosmogenic Radionuclides in Ice Cores. In: Encyclopedia of quaternary science, Mock, C. (Ed.), Elsevier, 2013.

Muscheler, R., Joos, F., Beer, J., Muller, S. A., Vonmoos, M., and Snowball, I.: Solar activity during the last 1000 yr inferred from radionuclide records, Quatern. Sci. Rev., 26, 82-97, 2007.

595   Petrenko, V. V., Severinghaus, J. P., Schaefer, H., Smith, A. M., Kuhl, T., Baggenstos, D., Hua, Q., Brook, E. J., Rose, P., Kulin, R., Bauska, T., Harth, C., Buizert, C., Orsi, A., Emanuele, G., Lee, J. E., Brailsford, G., Keeling, R., and Weiss, R. F.: Measurements of C-14 in ancient ice from Taylor Glacier, Antarctica constrain in situ cosmogenic (CH4)-C-14 and (CO)-C-14 production rates, Geochim. Cosmochim. Acta, 177, 62-77, 2016.

Petrenko, V. V., Severinghaus, J. P., Smith, A. M., Riedel, K., Baggenstos, D., Harth, C., Orsi, A., Hua, Q., Franz, P.,
600   Takeshita, Y., Brailsford, G. W., Weiss, R. F., Buizert, C., Dickson, A., and Schaefer, H.: High-precision C-14 measurements demonstrate production of in situ cosmogenic (CH4)-C-14 and rapid loss of in situ cosmogenic (CO)-C-14 in shallow Greenland firn, Earth Planet. Sci. Lett, 365, 190-197, 2013.

Petrenko, V. V., Smith, A. M., Crosier, E. M., Kazemi, R., Place, P., Colton, A., Yang, B., Hua, Q., and Murray, L. T.: An improved method for atmospheric (CO)-C-14 measurements, Atmos. Meas. Tech., 14, 2055-2063, 2021.

605   Petrenko, V., Neff, P., Etheridge, D., Smith, A., Buizert, C, Murray, L., Trudinger, C., Shi, M., Crosier, E., Hmiel, B., Thornton, D., Jong, L., van Ommen, T., Curran, M., Moy, A., Plummer, C., Nation, M., Beaudette, R., Harth,

Langenfelds, R., Mitrevski, B., Dyonisius, M., Ng, J., Severinghaus, J.P., Weiss, R.: Insights into the preindustrial atmospheric methane sources and sinks from $^{14}CH_4$ and ^{14}CO measurements at Law Dome, Antarctica. AGU Fall Meeting, 2023.

610 Poluianov, S., Kovaltsov, G.A. and Usoskin, I.G.: Solar energetic particles and galactic cosmic rays over millions of years as inferred from data on cosmogenic ^{26}Al in lunar samples, Astron. Astrophys., 618, A97, 2018.

Rogers, I. W. and Tristam, M.: The Absolute Depth Intensity Curve for Cosmic-Ray Muons Underwater and the Integral Sea-Level Momentum Spectrum in the Range 1-100 Gev/C, J. Phys. G Nucl. Phys., 10, 983-1001, 1984.

Smith, T., Cook, D. L., Merchel, S., Pavetich, S., Rugel, G., Scharf, A., and Leya, I.: The constancy of galactic cosmic 615 rays as recorded by cosmogenic nuclides in iron meteorites, Meteorit. Planet. Sci., 54, 2951-2976, 2019.

Steinhilber, F., Abreu, J. A., Beer, J., Brunner, I., Christl, M., Fischer, H., Heikkila, U., Kubik, P. W., Mann, M., McCracken, K. G., Miller, H., Miyahara, H., Oerter, H., and Wilhelms, F.: 9,400 years of cosmic radiation and solar activity from ice cores and tree rings, Proc. Nat. Acad. Sci. USA, 109, 5967-5971, 2012.

Steinhilber, F., Beer, J., and Frohlich, C.: Total solar irradiance during the Holocene, Geophys. Res. Lett., 36, 2009.

620 Thomas, B. C., Engler, E. E., Kachelriess, M., Melott, A. L., Overholt, A. C., and Semikoz, D. V.: Terrestrial Effects of Nearby Supernovae in the Early Pleistocene, Astrophys. J. Lett., 826, 2016.

Usoskin, I. G., Gallet, Y., Lopes, F., Kovaltsov, G. A., and Hulot, G.: Solar activity during the Holocene: the Hallstatt cycle and its consequence for grand minima and maxima, Astron. Astrophys., 587, 2016.

Usoskin, I.G.: A history of solar activity over millennia, Liv. Rev. Solar Phys., 20:2, 2023.

625 van de Wal, R. S. W., Meijer, H. A. J., de Rooij, M., and van der Veen, C.: Radiocarbon analyses along the EDML ice core in Antarctica, Tellus B, 59, 157-165, 2007.

van der Kemp, W. J. M., Alderliesten, C., van der Borg, K., de Jong, A. F. M., Lamers, R. A. N., Oerlemans, J., Thomassen, M., and van de Wal, R. S. W.: In situ produced C-14 by cosmic ray muons in ablating Antarctic ice, Tellus B, 54, 186-192, 2002.

630 Wallner, A., Feige, J., Kinoshita, N., Paul, M., Fifield, L. K., Golser, R., Honda, M., Linnemann, U., Matsuzaki, H., Merchel, S., Rugel, G., Tims, S. G., Steier, P., Yamagata, T., and Winkler, S. R.: Recent near-Earth supernovae probed by global deposition of interstellar radioactive Fe-60, Nature, 532, 69-72, 2016.

Wieler, R., Beer, J., and Leya, I.: The Galactic Cosmic Ray Intensity over the Past 10(6)-10(9) Years as Recorded by Cosmogenic Nuclides in Meteorites and Terrestrial Samples, Space Sci. Rev., 176, 351-363, 2013.

635 Willenbring, J. K. and von Blanckenburg, F.: Long-term stability of global erosion rates and weathering during late-Cenozoic cooling, Nature, 465, 211-214, 2010.

Wu, C. J., Usoskin, I. G., Krivova, N., Kovaltsov, G. A., Baroni, M., Bard, E., and Solanki, S. K.: Solar activity over nine millennia: A consistent multi-proxy reconstruction, Astron. Astrophys., 615, 2018a.

Wu, C. J., Krivova, N., Solanki, S.K. and Usoskin, I. G.: Solar total and spectral irradiance reconstruction over the 640 last 9000 years, Astron. Astrophys., 620, A120, 2018b.